An Effective Approach to Achieve a Spin Gapless Semiconductor–Half-Metal–Metal Transition in Zigzag Graphene Nanoribbons: Attaching A Floating Induced Dipole Field via π–π Interactions

Jia Guan, Wei Chen, Yafei Li, Guangtao Yu, Zhiming Shi, Xuri Huang,* Chiachung Sun, and Zhongfang Chen**

Under first-principles computations, a simple strategy is identified to modulate the electronic and magnetic properties of zigzag graphene nanoribbons (zGNRs). This strategy takes advantage of the effect of the floating dipole field attached to zGNRs via π–π interactions. This dipole field is induced by the acceptor/donor functional groups, which decorate the ladder-structure polydiacetylene derivatives with an excellent delocalized π-conjugated backbone. By tuning the acceptor/donor groups, –C≡C– number, and zGNR width, greatly enriched electronic and magnetic properties, e.g., spin gapless semiconducting, half-metallic, and metallic behaviors, with the antiferromagnetic–ferromagnetic conversion can be achieved in zGNRs with perfect, 57-reconstructed, and partially hydrogenated edge patterns.

1. Introduction

The successful fabrication of the once assumed impossible material graphene – a single layer of graphite – by Novoselov et al.[1,2] inaugurated a new era for 2D nanomaterials.[3–8] Graphene has unique and exceptional thermal, mechanical and electrical properties,[9–16] such as massless Dirac Fermion behavior,[11,12] high mobility,[14,15] and the largest strength measured so far.[16] These appealing properties naturally stimulated extensive experimental and theoretical investigations on graphene-based materials,[17–45] particularly 1D graphene nanoribbons (GNRs),[30–45] which can be realized by cutting 2D graphene.[14,43,44]

Dr. J. Guan, Prof. W. Chen, Prof. G. T. Yu
Dr. Z. M. Shi, Prof. X. R. Huang, Prof. C. C. Sun
The State Key Laboratory of Theoretical and Computational Chemistry
Institute of Theoretical Chemistry
Jilin University
Changchun 130023, P. R. China
E-mail: yugt@jlu.edu.cn; xurihuang09@gmail.com
Dr. Y. F. Li, Prof. Z. F. Chen
Department of Chemistry
Institute for Functional Nanomaterials
University of Puerto Rico
Rio Piedras Campus, San Juan, 00931, Puerto Rico
E-mail: zhongfangchen@gmail.com

DOI: 10.1002/adfm.201201677

GNRs exhibit vastly different properties from graphene.[30–46] Theoretical studies predict that H-terminated GNRs with either armchair or zigzag edges have non-zero band-gaps,[34–36] which has been experimentally confirmed.[37,38] Armchair GNRs (aGNRs) are nonmagnetic, while zigzag GNRs (zGNRs) are magnetic due to the localized edge states,[36,39,40] which are ferromagnetically ordered at each edge but antiferromagnetically coupled between the two edges.

Great endeavors have been made on functionalizing GNRs to tune the electronic and magnetic properties of pristine GNRs for their applications of multi-functional nanodevices.[46–70] Among others, the most intriguing discoveries are probably the realization of spin gapless semiconducting (SGS) and half-metallic behaviors in zGNRs, since these captivating properties make them superior candidates for spintronic applications.[40,56–68]

Spin gapless semiconducting (SGS) behavior was proposed by Wang,[52,53] and has been verified in doped $PbPdO_2$.[54,55] Such SGS materials could have four typical band configurations with either quadratic or linear energy-momentum dispersions, in which at least one of the spin channels in the valence bands touches the spin channels in the conduction bands at the Fermi level, or vice versa. However, few reports on achieving SGS in GNRs are available. Recently, Li et al. theoretically predicted that selective N-doping can realize SGS in zGNRs.[56] As another appealing feature, half-metallicity is the peculiar state with the coexistence of metallic behavior for electrons in one spin and insulating behavior in the other. Theoretically, Son et al. pioneered the idea of driving zGNRs into half-metal by applying a transverse electric field across the width.[40] Motivated by this study, researchers proposed several approaches to realize half-metallicity by chemical functionalizations, which can produce an internal potential difference between the zGNR edges similar to that by applying an external electric field.[56–67] For example, Kan et al.[57] and Zeng's group[58] demonstrated the edge-decoration induces half-metallic behavior with functional groups of NO_2/CH_3, SO_2/OH, and NO_2/OH pairs. Moreover, B-substitution[59] and selective N-doping can also give rise to half-metallicity in zGNRs.[56]

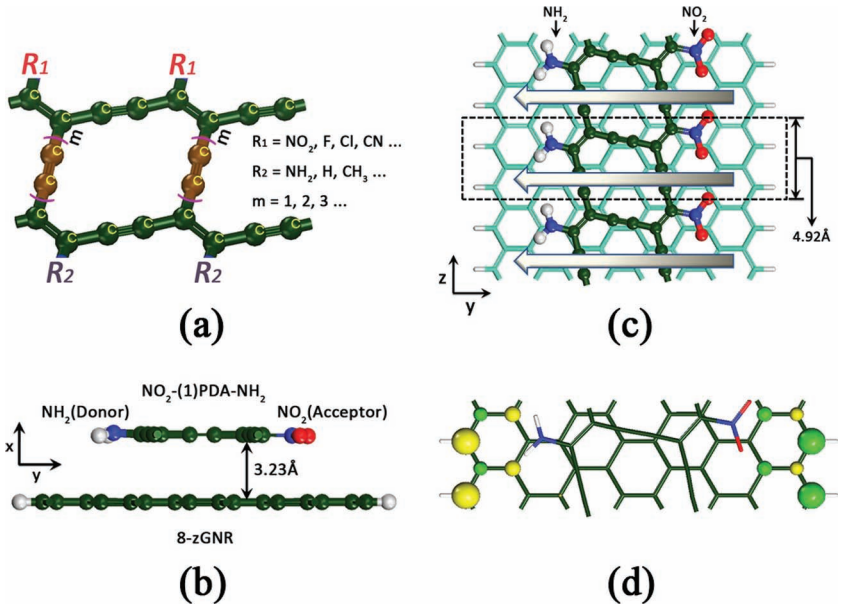

Figure 1. a) Structure of the double-chain ladder-like PDA derivatives. b) Optimized structure of *8*-NO_2-(*1*)PDA-NH_2. The PDA and zGNR are set parallel along the *z*-axis, and they are homocentric. c) Top view of the structure in panel b. The PDA is displayed in ball-and-stick style, while the 8-zGNR is in stick style. The arrows indicate the direction of the dipole moment induced by PDA (from the acceptor side to the donor side). The part in the dashed line corresponds to one unit cell. d) Top view of spatial spin distribution of *8*-NO_2-(*1*)PDA-NH_2 within one unit cell.

Different from the above in-plane/covalent modifications,[40,56–67] another promising approach for endowing zGNRs the potentials of half-metallicity and possibly also spin gapless semiconductor for spintronic applications is by surface modification via noncovalent interactions.[68] This approach has several advantages, among others, it is simple and multi-optional, and most importantly, almost no defects or strong structural deformations may occur and the delocalized π-conjugation in zGNRs is nearly undisrupted. A noteworthy report by Lee et al.[68] is that adsorbing multiple ferroelectric poly(vinylidene fluoride) (PVDF) polymers can realize half-metallicity in zGNRs. Besides inducing half-metallicity,[68] surface modification is expected to tailor the band-gaps of zGNRs,[69,70] although the SGSs have not been reported yet. For example, Alexas and coworkers proposed that the adsorption of the π-conjugated polymer PmPV can slightly decrease/increase the band-gaps of zGNRs/aGNRs through the π–π interaction.[70]

Inspired by these studies, in this work, we proposed a new strategy to modulate the electronic and magnetic properties of zGNRs by the floating induced dipole field attached to the nanoribbons via simple π–π interactions. This dipole field is induced by the acceptor/donor functional groups which are decorating ladder-structure polydiacetylene (PDA) derivatives. In this structure, the two chains of PDA derivatives, serving as an excellent delocalized π-conjugated backbone, are functionalized by regularly arranged electron-acceptor and donor groups, respectively, which are linked with the versatile –C≡C– bonds (**Figure 1**a). The electron transfer from donor to acceptor groups introduces dipole moments, which can be further enhanced by elongating the –C≡C– chains (Figure 1c). It is expected that this type of floating dipole field induced by PDA derivatives can produce potential differences between the edges of zGNRs and drive zGNRs into half-metal, even provide other appealing electronic features, e.g., spin gapless semiconductor, by changing the –C≡C– number of the PDA bridges. Note that PDA and its –C≡C– bridged ladder-structure derivatives have been synthesized experimentally,[71–75] and a PDA layer adhered on the graphene surface has been fabricated recently as a bimorph actuator with compelling advantages to the traditional electromechanical actuation technology,[76] and the electronic couplings of PDA nanowires on graphite have also been experimentally studied.[77–79] Moreover, the NO_2/NH_2 decorated ladder-structure PDA derivatives linked with one –C≡C– bond were predicted to exhibit significantly enhanced nonlinear optical (NLO) responses due to the excellent π-conjugated delocalization of the PDA backbone.[80]

Here, we perform comprehensive density functional theory (DFT) computations to investigate the electronic and magnetic properties of the joint systems of zGNR and the decorated PDA derivatives, emphasizing the effects of different pairs of acceptor/donor groups, number of –C≡C– bonds in the PDA derivatives and the zGNR width, even the existence of edge 57-reconstruction in zGNRs. Our studies revealed that depositing the decorated PDA derivatives on perfect H-terminated zGNRs renders the joint systems the transition of SGS–half-metal–metal, accompanied by the magnetic conversion from AFM to FM. Even with the existence of 57-reconstruction at the zGNR edges, abundant electronic and magnetic transitions of AFM SGS–FM half-metal–AFM metal–NM metal can also be observed in the joint systems. Moreover, through partially hydrogenating zGNRs at the 57-reconstructed edges, the effect of the edge reconstruction can be eliminated, and more fascinatingly, the electronic and magnetic properties of the joint systems based on edge-reconstructed wide zGNRs can be generally recovered to those of the corresponding joint systems with perfect narrow H-terminated zGNRs representing the remaining pristine zGNRs inside.

These provide immensely valuable insights for facilitating the spintronic applications and effectively modulating the electronic and magnetic properties of zGNR-based nanomaterials with the unitary PDA derivative polymer.

2. Results and Discussion

2.1. Geometries, Electronic and Magnetic Properties of Joint Systems of Perfect H-Terminated zGNRs and Decorated PDA Derivatives

In this section, we examine the effects of different acceptor/donor groups and linker lengths in the decorated PDA deriva-

Table 1. The relative energies (meV) of different magnetic couplings to the ground state per unit, formation energies (meV) per unit and the corresponding electronic properties of the ground states of the joint systems of *8*-acceptor-(*1*)PDA-donor (acceptor/donor = NO_2/NH_2, F/H, Cl/H, and CN/CH_3). NM, FM, and AFM here represent the nonmagnetic, ferromagnetic, and antiferromagnetic spin couplings, respectively.

System	NM [meV]	FM [meV]	AFM [meV]	E_f [meV]	Electronic property
8-NO_2-(*1*)PDA-NH_2	98.0	16.4	0.0	–815.5	half-metal
8-F-(*1*)PDA-H	124.8	1.6	0.0	–559.9	metal
8-Cl-(*1*)PDA-H	128.0	2.5	0.0	–583.8	metal
8-CN-(*1*)PDA-CH_3	115.4	0.0	9.6	–775.2	metal

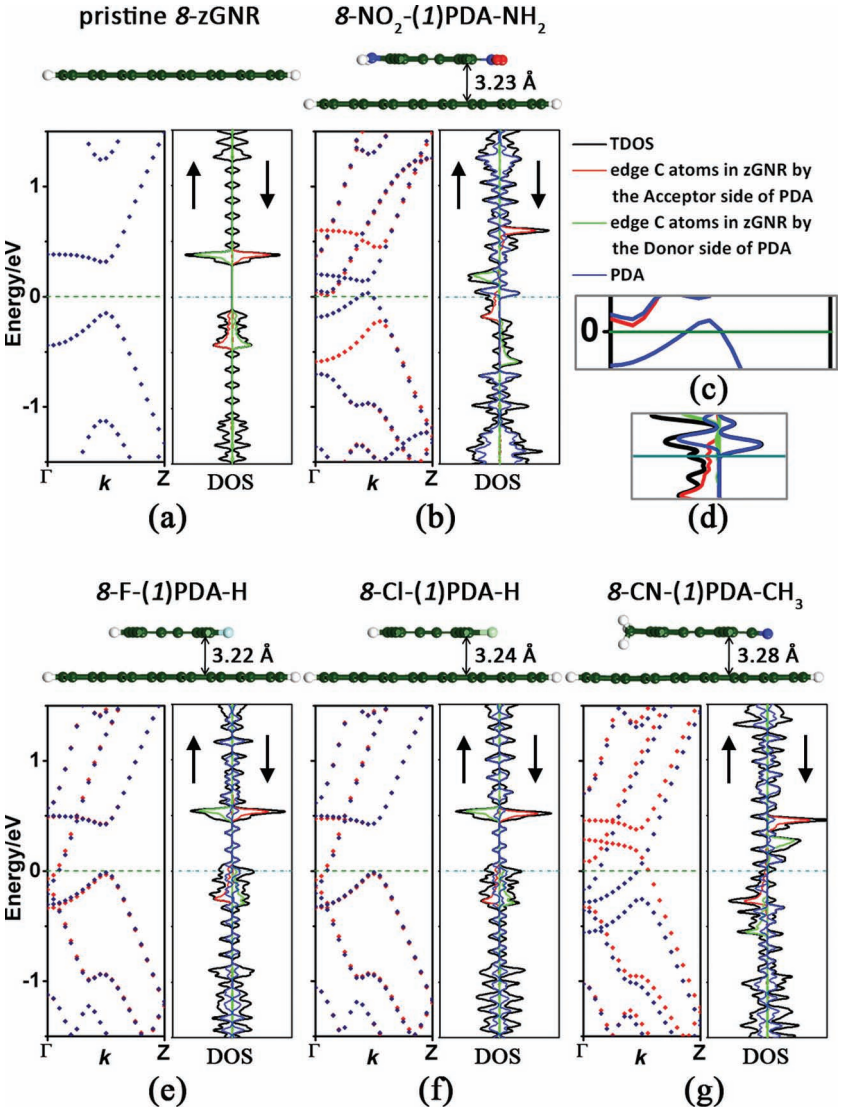

Figure 2. Equilibrium geometries, band structures and DOSs of pristine 8-zGNR and the joint systems of 8-zGNR and PDA derivatives decorated with four different acceptor/donor pairs. The blue and red plots denote the spin-up (↑) and spin-down (↓) channels for the band structures, respectively. The Fermi level is set as zero and marked with a green dashed line. c,d) The zooms on the region around Fermi-level in the band structure and DOS of (b).

tives and the width of H-terminated zGNR with smooth edges. The joint system of zGNR and the decorated PDA is named as *n*-acceptor-(*m*)PDA-donor, where *n* is the width of zGNR, *m* and acceptor/donor denote the number of –C≡C– bonds in the linking bridge and the pair of edge functional groups in the PDA derivatives, respectively. We will begin from 8-zGNR as an example, and then go to study perfect zGNRs with different widths.

2.1.1. 8-Acceptor-(1)PDA-Donor

First, we investigated the joint system of *8*-NO_2-(*1*)PDA-NH_2 (Figure 1b), in which the two PDA chains are decorated by the NO_2/NH_2 groups and linked by one –C≡C– bond, and the 8-zGNR serves as the supporting system. To obtain the ground state of *8*-NO_2-(*1*)PDA-NH_2, we considered three spin configurations, namely nonmagnetic (NM), ferromagnetic (FM), and antiferromagnetic (AFM). Our computations showed that AFM is the ground state (energetically more favorable than NM and FM by 98.0 and 16.4 meV, respectively; **Table 1**), and the corresponding equilibrium distance between the planes of 8-zGNR and NO_2-(1)PDA-NH_2 is about 3.23 Å. To obtain further insight into the magnetism of *8*-NO_2-(*1*)PDA-NH_2, we computed the corresponding spin density distribution (Figure 1d), which reveals that the unpaired spin mainly concentrates on the edge C atoms of 8-zGNR. These edge C atoms of zGNRs should be responsible for the magnetic behavior of the joint systems.

Interestingly, *8*-NO_2-(*1*)PDA-NH_2 exhibits a typical half-metallic behavior, i.e., the energy level in the spin-up channel crosses the Fermi-level, while the energy levels in the spin-down channel do not (**Figure 2**b).

To understand the origin of the half-metallic band structure, we plotted the total density of states (TDOS) and local density of states (LDOS) of *8*-NO_2-(*1*)PDA-NH_2. Obviously, the state crossing the Fermi-level arises from the edge carbon atoms of 8-zGNR, mainly from those at the NO_2 side (Figure 2d). Clearly, the NO_2/NH_2 decoration breaks the twofold degenerated flat bands of the edge states in the perfect 8-zGNR around the Γ point, and the top valence band in the spin-up channel is shifted across the Fermi-level (Figure 2a,b), which results in half-metallicity.

Naturally, we wondered whether PDAs decorated by other different acceptor/donor groups could also lead to the similar electronic and magnetic behaviors in 8-zGNR, such as half-metallicity. Thus, we selected three other acceptor/donor pairs, namely F/H, Cl/H, and CN/CH_3, as typical examples to address this issue.

Table 2. The relative energies (meV) of different magnetic couplings to the ground state per unit, formation energies (meV) per unit and the corresponding electronic properties of the joint systems of *n*-NO_2-(*1*)PDA-NH_2 (*n* = 4, 8, 10, 12, 14).

System	NM [meV]	FM [meV]	AFM [meV]	E_f [meV]	Electronic property
4-NO_2-(*1*)PDA-NH_2	51.0	0.0	8.6	−627.3	metal
8-NO_2-(*1*)PDA-NH_2	98.0	16.4	0.0	−815.5	half-metal
10-NO_2-(*1*)PDA-NH_2	125.1	10.3	0.0	−890.5	SGS
12-NO_2-(*1*)PDA-NH_2	146.0	5.1	0.0	−851.0	SGS
14-NO_2-(*1*)PDA-NH_2	138.5	3.8	0.0	−876.7	SGS

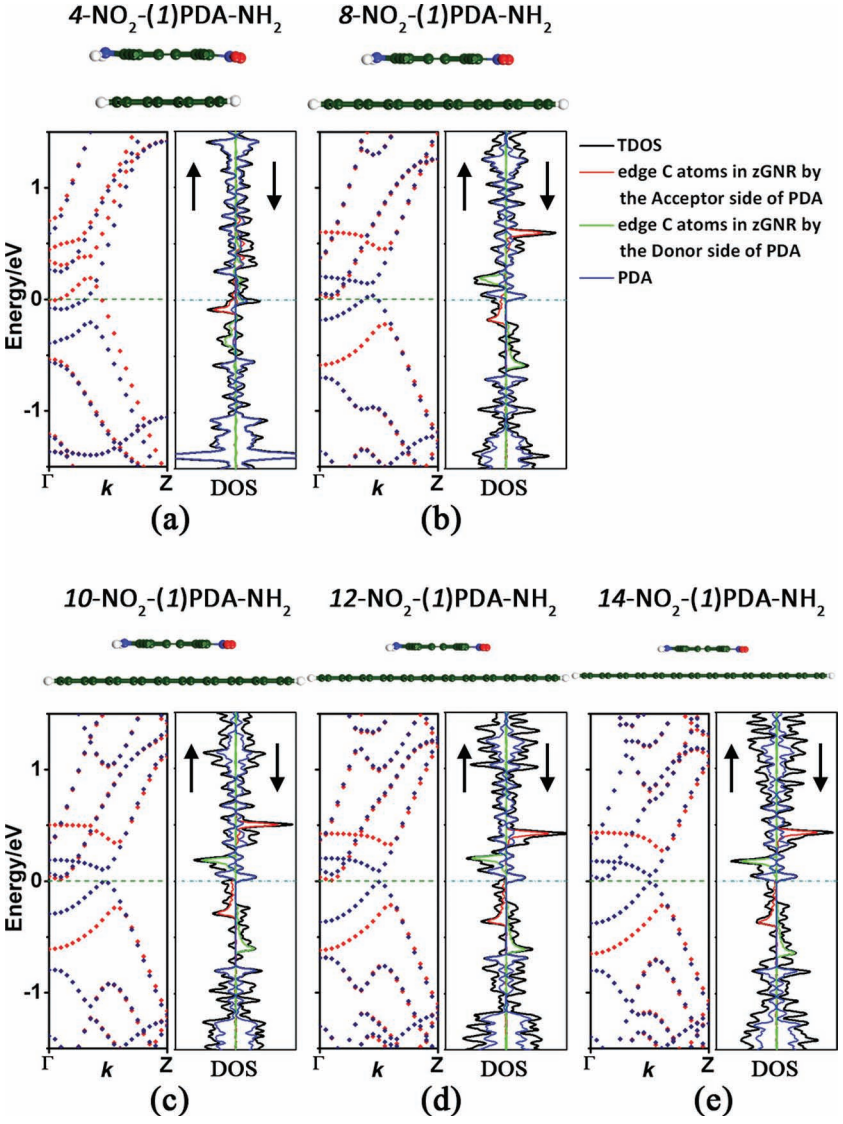

Figure 3. Equilibrium geometries, band structures and DOSs of *n*-NO_2-(*1*)PDA-NH_2 (*n* = 4, 8, 10, 12, 14). The blue and red plots denote the spin-up (↑) and spin-down (↓) channels for the band structures, respectively. The Fermi level is set as zero and marked with a green dashed line.

Our computations found that the ground states for *8*-F-(*1*)PDA-H and *8*-Cl-(*1*)PDA-H are AFM, while that for *8*-CN-(*1*)PDA-CH_3 is FM, and the corresponding equilibrium distances between the planes of 8-zGNR and PDA derivatives are about 3.22, 3.24, and 3.28 Å, respectively. Different from the half-metallicity of *8*-NO_2-(*1*)PDA-NH_2, all these three joint systems, *8*-F-(*1*)PDA-H, *8*-Cl-(*1*)PDA-H and *8*-CN-(*1*)PDA-CH_3, exhibit metallic behavior, and their DOSs reveal that the metallic behaviors originate from both the edge carbon atoms in 8-zGNR and the PDA derivatives (Figure 2e–g).

Evidently, decorating the PDAs by different acceptor/donor groups can effectively modulate the electronic property of 8-zGNR: the semiconducting 8-zGNR has been transformed into half-metal by decorating NO_2/NH_2, and into metal when F/H, Cl/H, and CN/CH_3 are used to functionalize PDAs. Note that several methods have been proposed to realize half-metallicity in zGNRs, such as by applying external electric field,[40] edge functionalization[57,58,60] and substitution of designated carbon atoms.[56,59] Depositing the PDA derivative decorated by NO_2/NH_2 is a new and simple way to achieve half-metallicity through the induced dipole field via π–π interactions.

Due to the unique ability of the NO_2/NH_2 functionalization to transfer 8-zGNR into half-metal, we will focus on this PDA functionalization in the remaining sections of this work. It is very likely that the electronic and magnetic properties of the joint systems of zGNR and NO_2-PDA-NH_2 can be tuned by modulating the zGNR width and the number of –C≡C– bonds in the linking bridge of NO_2-PDA-NH_2. Thus, in the next section, we will mainly examine these effects, especially whether the half-metallicity will be maintained, how the electronic and magnetic properties of the joint systems will be affected, e.g., inducing some appealing properties like SGS, as narrowing/widening the widths of zGNR or increasing the –C≡C– number.

2.1.2. *n*-NO_2-(*m*)PDA-NH_2

We investigated the joint systems of *n*-NO_2-(*m*)PDA-NH_2 (*n* = 4, 10, 12, 14; *m* = 1, 2, 3) to examine the effects of zGNR widths and –C≡C– number in the linking bridge of NO_2-PDA-NH_2 on the electronic and magnetic properties of the joint systems.

Firstly, we studied the systems of *n*-NO_2-(*1*)PDA-NH_2 (*n* = 4, 10, 12, 14) with one –C≡C– bond as the linking bridge in NO_2-PDA-NH_2. As illustrated in **Table 2** and **Figure 3**, when the width *n* of zGNR is narrowed from 8 to 4, the corresponding electronic behavior is transformed from half-metal into metal, accompanied by the magnetic conversion from AFM to FM. The computed DOS reveals that the degenerated edge states in the

pristine semiconducting 4-zGNR are broken by NO_2-(1)PDA-NH_2, and the according energy levels from both the spin-up and the spin-down channels are driven across the Fermi-level, resulting in the metallic behavior contributed by both the edge carbon atoms of 4-zGNR and the NO_2-(1)PDA-NH_2 (Figure 3a).

On the contrary, when 8-zGNR is elongated to 10-zGNR, the corresponding half-metallic behavior of the joint system is changed into spin gapless semiconducting feature (Figure 3c), while preserving the AFM magnetism. As further increasing the width *n* of zGNR into 12 and 14, the AFM state and SGS behavior are sustained in *12*-NO_2-(*1*)PDA-NH_2 (Figure 3d) and *14*-NO_2-(*1*)PDA-NH_2 (Figure 3e). In all of these three semiconducting systems, the degenerated edge states of the pristine zGNRs are broken when NO_2-(1)PDA-NH_2 is deposited, with both the top valence band from the up-spin edge state of the corresponding zGNR and the bottom conduction band from the impurity state of PDA touching the Fermi-level, which results in the SGS behaviors, as illustrated in the three computed DOSs (Figure 3).

Remarkably, the deposition of NO_2-PDA-NH_2 with one –C≡C– bond as the linking bridge on zGNR has rendered abundant transformations of the electronic and magnetic properties in the corresponding joint systems: as increasing the width *n* of semiconducting zGNRs, the transition of metal–half-metal–spin gapless semiconductor is observed in *n*-NO_2-(*1*)PDA-NH_2 (*n* = 4, 8, 10, 12, 14), along with the magnetic conversion from FM to AFM. This can be attributed to the fact that the effect of the induced dipole field by NO_2-(1)PDA-NH_2 decays as increasing the width *n* of the zGNR.

Considering the effect of the induced dipole field, we naturally intend to investigate the effect of the –C≡C– number on the electronic and magnetic properties of the joint systems, since the more –C≡C– bonds, the more delocalized π-conjugation and the stronger induced dipole field. Subsequently, we investigated the joint systems of *n*-NO_2-(*2*)PDA-NH_2 (*n* = 8, 10, 12, 14), in which NO_2-PDA-NH_2 has two –C≡C– bonds as the linking bridge.

As increasing the –C≡C– number from one to two (strengthening the induced dipole field), *8*-NO_2-(*2*)PDA-NH_2 sustains the AFM and half-metallic behavior. However, different from *8*-NO_2-(*1*)PDA-NH_2, the computed DOS shows that the half-metallicity in *8*-NO_2-(*2*)PDA-NH_2 arises from both the edge carbon atoms of 8-zGNR and NO_2-(2)PDA-NH_2 (**Figure 4**b). When the width *n* of zGNR is increased into 10, the corresponding electronic feature of the joint systems is driven from SGS (*10*-NO_2-(*1*)PDA-NH_2) into half-metal (*10*-NO_2-(*2*)PDA-NH_2) while remaining in the AFM ground state. The DOS analysis reveals that the half-metallicity is mainly contributed by the edge carbon atoms in 10-zGNR at the NO_2 side (Figure 4e). As the zGNR is further elongated into 12-zGNR and 14-zGNR, the joint systems preserve SGS character with AFM state in *12*-NO_2-(*2*)PDA-NH_2 and *14*-NO_2-(*2*)PDA-NH_2 (Figure 4h,k). Both DOSs reveal that the SGSs originate from the edge carbon atoms in zGNRs at the NO_2 side and the impurity state of PDA.

When the –C≡C– number in the linking bridges is further increased into three, the induced dipole field in NO_2-(3)PDA-NH_2 gets even more strengthened. Consequently, the corresponding electronic feature of the joint systems is driven from the half-metallic *8*-NO_2-(*2*)PDA-NH_2 into metallic

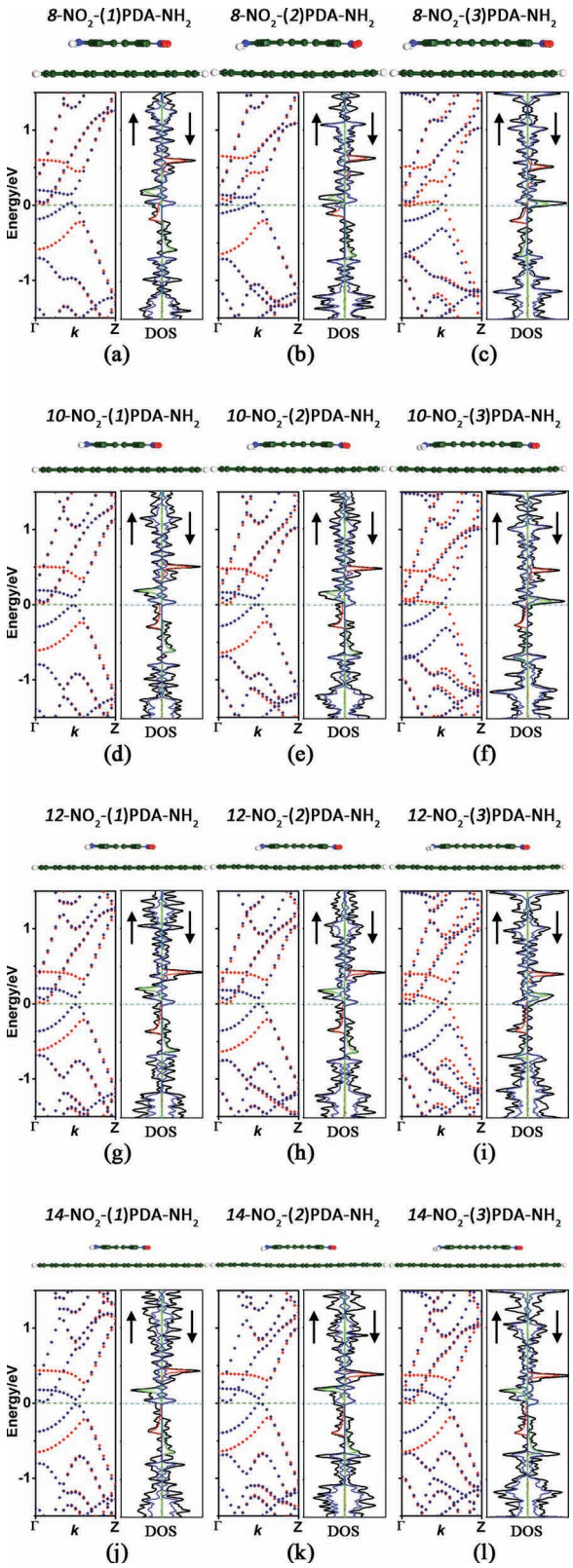

Figure 4. Equilibrium geometries, band structures and DOSs of *n*-NO_2-(*m*)PDA-NH_2 (*n* = 8, 10, 12, 14; *m* = 1, 2, 3). The blue and red plots denote the spin-up (↑) and spin-down (↓) channels for the band structures, respectively. The Fermi level is set as zero and marked with a green dashed line.

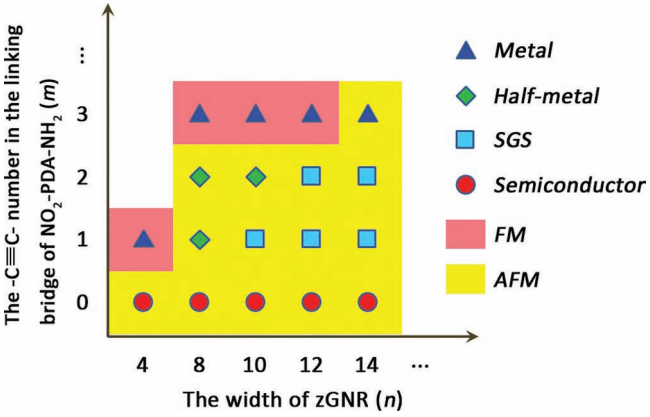

Figure 5. The effects of zGNR width and –C≡C– number in the linking bridge on the electronic and magnetic behaviors of the joint systems *n*-NO_2-(*m*)PDA-NH_2 (*n* = 4, 8, 10, 12, 14; *m* = 1, 2, 3).

8-NO_2-(*3*)PDA-NH_2, with the magnetic conversion from AFM to FM state. The computed DOS shows that the metallicity originates from both the edge carbon atoms of 8-zGNR and NO_2-(3)PDA-NH_2 (Figure 4c). A similar transition from AFM half-metal to FM metal is also observed for the wider 10-zGNR, with the same origination of the metallicity of *10*-NO_2-(*3*)PDA-NH_2 (Figure 4f). When the width *n* of zGNR is further increased into 12 and 14, the *12*-NO_2-(*3*)PDA-NH_2 and *14*-NO_2-(*3*)PDA-NH_2 are directly transformed into metal (Figures 4i,l), and *12*-NO_2-(*3*)PDA-NH_2 converts from AFM to FM while *14*-NO_2-(*3*)PDA-NH_2 maintains AFM. The respective DOSs show that the edge carbon atoms of 12-zGNR and NO_2-(3)PDA-NH_2 contribute to the metallicity of *12*-NO_2-(*3*)PDA-NH_2; differently, the metallicity of *14*-NO_2-(*3*)PDA-NH_2 originates from the edge carbon atoms of 14-zGNR at the NO_2 side and the impurity state of PDA.

Figure 5 summarizes the electronic and magnetic behaviors of the joint systems *n*-NO_2-(*m*)PDA-NH_2 that vary with the zGNR widths and the –C≡C– number in the linking bridge. Comparing with the pristine semiconducting zGNRs with smooth edges, evidently, by changing the width *n* of zGNR or altering the number *m* of –C≡C– bonds in the linking bridge, we can achieve the abundant electronic transformation of spin gapless semiconductor–half-metal–metal and the magnetic conversion of AFM and FM state in *n*-NO_2-(*m*)PDA-NH_2.

In retrospect to previous studies, several strategies have been proposed to achieve the appealing features of half-metallicity and spin gapless semiconductor in zGNRs, but their realization still remains greatly challenging. For example, by applying transverse electric field,[40] an onset electric field of stronger than 0.168 V $Å^{-1}$ is required to drive 8-zGNR half-metallic, which is not easy to realize under ordinary experimental conditions.[68] Moreover, through edge-decoration[57,58] and selective atom-substitution[56,59], zGNRs can be rendered SGS or half-metal, but the prerequisite to fine-control the location of the functional groups or designated atoms would also be harsh.[46,68]

Comparatively, surface modification is simple, and zGNRs as the supporting system essentially preserve the electronic and geometric integrity with no remarkable destruction. Notably, Lee et al.[68] predicted that weakly binding the multiple aligned PVDF polymers to the surface of zGNRs would be able to drive zGNRs half-metallic, due to the effect of the dipole field induced through the σ-charge transfer from H side to the F side in PVDFs; however, multiple PVDFs have to be used to generate a dipole field strong enough, since a single PVDF can just slightly narrow the band-gap of zGNRs.

Our proposition also belongs to the family of surface modification, but has several unique advantages. First, this strategy renders much stronger induced dipole field, consequently, the unitary acceptor/donor decorating PDA derivative can achieve half-metallicity in zGNRs without the aid of external electric field. This is because in our systems the dipole moments are introduced via the electron-transfer from the donor to the acceptor groups through the excellent delocalized π-conjugated backbone of the PDA derivatives, where the π-electrons have much better mobility. Second, strong π–π interactions exist between the PDA derivative and zGNR (see Section 2.3), which is advantageous for experimental realization. Third, besides half-metallicity, another superior feature, namely spin gapless semiconductor, can also be realized in zGNRs, even the prolific electronic transition of spin gapless semiconductor–half-metal–metal with the magnetic conversion from AFM to FM state can be achieved. This is the first report on realizing the abundant transitions of the electronic and magnetic behaviors in zGNRs by means of the surface modification strategy based on the floating induced dipole moment.

2.2. The Electronic and Magnetic Properties of the Joint Systems of NO_2-(1)PDA-NH_2 and zGNR with 57-Reconstructed Edges

All of the above joint systems under study focused on the zGNRs with H-termination, which serves as a popular passivation to saturate the edge dangling bonds of the unpassivated zGNRs. Such H-terminated zGNRs with smooth edges have been extensively employed as models to study functionalized zGNRs,[40,56–70] e.g., applying transverse electric field across zGNRs width,[40] substituting designated C atoms with B/N atoms,[56,59] or noncovalently physisorbing multiple PVDFs chains[68]/$NH_3(CH)_6CO_2$ molecule[69] on zGNRs to tailor the band-gap, even to induce the intriguing half-metallic or SGS behaviors.

On the other hand, the bare zigzag edges of zGNRs may not be smooth, especially they are vulnerable to the deformation of 57-reconstruction, as observed experimentally.[81–83] Not surprisingly, theoretical efforts have been tempted on the edge 57-reconstruction in zGNRs, and revealed that formation of the 57-reconstruction at the edge(s) can significantly affect the electronic and magnetic behaviors of zGNRs.[49–51,84–87] For example, Kunstmann et al. revealed that zGNRs with both fully 57-reconstructed edges exhibit metallic behavior with nonmagnetic state, regardless of the edges unpassivated or H-terminated,[51] while Sudipta et al. found that a line of 57-reconstructions along one edge of H-terminated zGNRs can suppress the edge magnetism and induce metallic behavior.[49] Thus, we decided to investigate the effect of 57-reconstruction on the zGNRs edges.

2.2.1. The Joint Systems of NO_2-(1)PDA-NH_2 and Unpassivated/H-Terminated zGNRs with 57-Reconstructed Edge(s)

Several important questions rise naturally when the edge 57 reconstructions occur: how will such reconstructions affect the electronic and magnetic properties of the joint systems of PDA and zGNRs? Can the appealing features, e.g., half-metallicity and SGS, survive in the joint systems containing the zGNRs with 57-reconstructed edge(s)?

In this work, we took 14-zGNR as an example, and considered four typical patterns of 57-reconstruction at the zGNR edge(s) in the joint systems, namely, intervallic perfect hexagon pair and pentagon-heptagon pair (denoted by "*i*") at single edge and both edges, and full 57-reconstruction (denoted by "*f*") at single edge and both edges. The corresponding joint systems are labeled as *-14*-zGNR-*i*57S, *-14*-zGNR-*i*57D, *-14*-zGNR-*f*57S, and *-14*-zGNR-*f*57D, respectively, where *14* and 57 represent ribbon width and 57-reconstruction, and S and D mean single and both edge(s), respectively. Here, edge 57-reconstructed 14-zGNRs with both unpassivated and H-terminated edges are considered, and they are differentiated by marking with the labels of "*e*b" and "*e*H", respectively. Moreover, perfect H-terminated zGNRs are referred to as "H-N_z-zGNR", where N_z is the ribbon width. Note that the PDA employed in the joint systems based on the zGNRs with edge 57-reconstruction is the NO_2/NH_2 decorated ladder-structure PDA with one –C≡C– bond as the linkers (NO_2-(1)PDA-NH_2).

Our computational results are exciting: similar to the corresponding joint structure based on H-*14*-zGNR with smooth edges, the AFM SGS feature can be observed in *e*b-*14*-zGNR-*i*57D where intervallic 57-reconstructions occur at both edges of bare 14-zGNR (**Figure 6**b); when intervallic 57-reconstruction merely occurs at single edge of bare 14-zGNR, the SGS behavior of the joint system can be converted to the intriguing

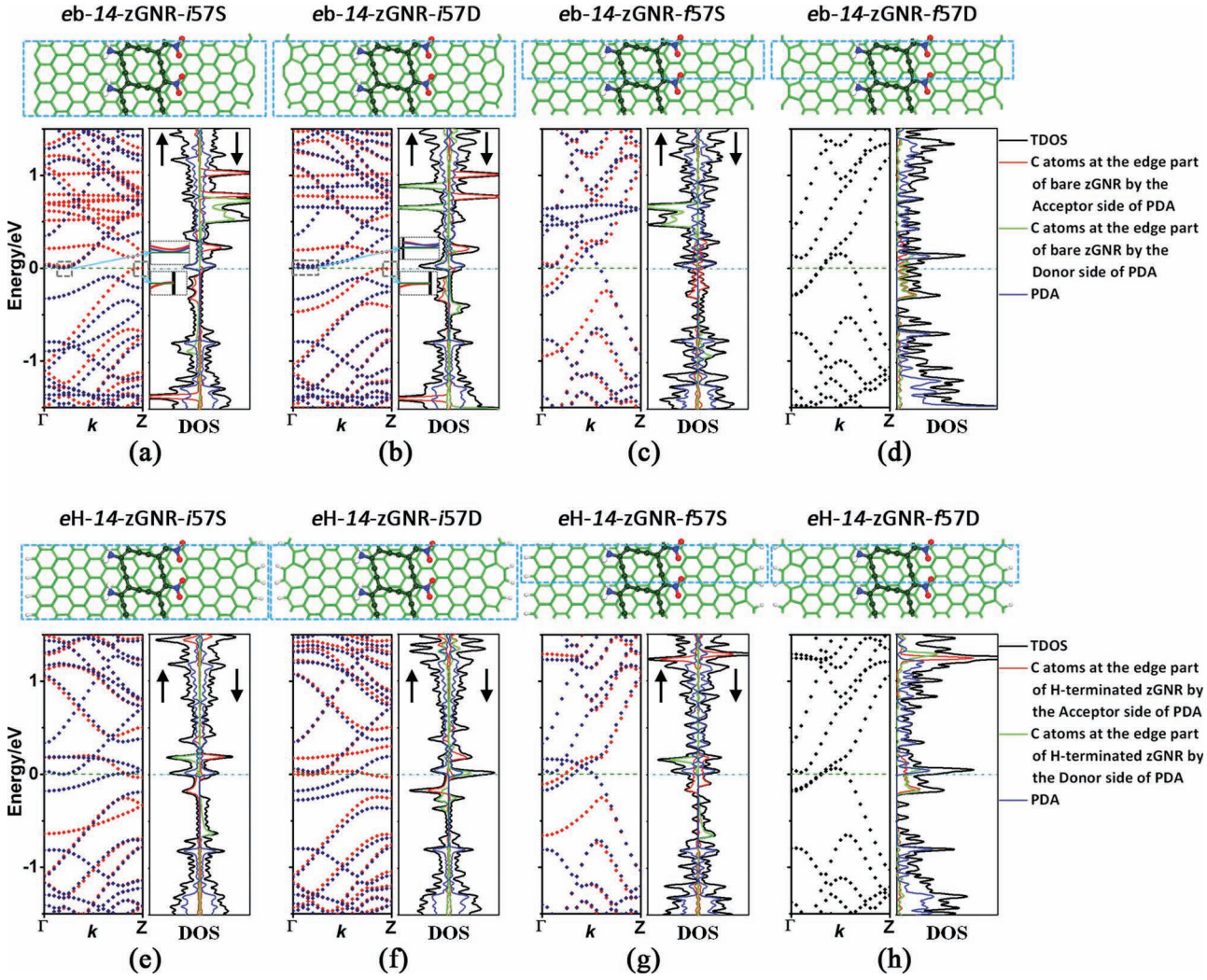

Figure 6. Equilibrium geometries, band structures and DOSs of the joint systems of NO_2-(1)PDA-NH_2 and unpassivated/H-terminated 14-zGNRs with single/both edge(s) partially/continuously 57-reconstructed. The blue and red plots denote the spin-up (↑) and spin-down (↓) channels for the spin-polarized band structures in (a–c,e–g). The Fermi level is set as zero and marked with a green dashed line. The band behaviors about the Fermi-level in (a,b) are zoomed in to make them clearer. The parts in the blue dotted line correspond to one unit cell.

half-metallicity in *e*b-*14*-zGNR-*i*57S (Figure 6a), accompanied by the magnetic conversion from AFM to FM. The respective computed DOS results reveal that the SGS arises from the C atoms at both edges of bare 14-zGNR and the impurity state of PDA (Figure 6b), whereas the half-metallic behavior is mainly contributed by the C atoms at the edge of bare 14-zGNR at the NO_2 side of PDA (Figure 6a). Further, when single/both edge(s) of the bare 14-zGNR are fully 57-reconstructed (Figure 6c,d), the joint systems can be driven into metal with AFM/NM state, respectively. It is the C atoms at the edge of bare 14-zGNR at the NO_2 side of PDA that contribute to the metallicity of *e*b-*14*-zGNR-*f*57S, whereas that of *e*b-*14*-zGNR-*f*57D originates from the C atoms at both edges, as shown in their computed DOSs (Figure 6c,d). Obviously, abundant electronic and magnetic transitions of AFM SGS–FM half-metal–AFM metal–NM metal can be obtained in the joint systems of NO_2-(1)PDA-NH_2 and bare 14-zGNRs with 57-reconstructed edge(s).

In order to make more detailed comparisons, we further investigated the corresponding joint systems of NO_2-(1)PDA-NH_2 and H-terminated 14-zGNRs with these four types of edge reconstruction, which can be viewed as the structural analogues of H-terminated 14-zGNR with smooth edges. We found that H-termination at the zGNR edge(s) with intervallic 57-reconstructions can lead to the transformation from the half-metallicity and SGS of both parallel unpassivated-joint-systems (*e*b-*14*-zGNR-*i*57S and *e*b-*14*-zGNR-*i*57D) into metal with AFM and FM states, respectively (Figure 6e,f). In contrast, with single/both edge(s) fully 57-reconstructed, the corresponding joint systems are still metallic with AFM/NM state, similar to the cases with their correlative bare zGNRs with 57-reconstruction (Figure 6g,h). The computed DOSs reveal that all of the metallic behaviors in these four joint systems of PDA and H-terminated 14-zGNR with edge(s) 57-reconstructed are mainly contributed by the C atoms at both edges of 14-zGNRs and PDA. Clearly, for the H-terminated 14-zGNRs with edge(s) 57-reconstructed, all of four joint systems are driven metallic unanimously, different from the AFM SGS behavior of the related analogue based on H-terminated 14-zGNR with smooth edges.

Finally, comparing these eight joint systems of PDA and unpassivated/H-terminated 14-zGNRs with edge(s) 57-reconstructed, we can observe that continuous 57-reconstruction at the edge(s) impacts the electronic and magnetic properties of the joint systems more prominently, even resulting in the disappearance of the magnetism in the fully reconstructed edge(s), in contrast to the remnant of magnetism with partial reconstruction.

2.2.2. The Joint Systems of NO_2-(1)PDA-NH_2 and Partially Hydrogenated zGNRs at the 57-Reconstructed Edge(s)

As we know, 57-reconstruction at the edge(s) can significantly impact the electronic and magnetic properties of zGNRs.[49–51,84–87] However, Xiang et al.'s fascinating work[48] revealed that partially hydrogenating wider zGNRs at not only smooth but also reconstructed edges can render similar electronic and magnetic properties to the corresponding perfect narrow H-terminated zGNR that represents the remaining zGNR inside, thus is an effective and very promising approach to realize "narrow" GNRs with smooth edges.

Motivated by this interesting finding, we wonder whether the electronic and magnetic features of the joint systems of PDA and edge-reconstructed zGNRs can be recovered by partially hydrogenating zGNRs at the reconstructed edges. Thus, we investigated the effect of partial hydrogenation at the reconstructed edges on the corresponding electronic and magnetic characteristics, and in particular, examined whether the electronic and magnetic features of the joint systems with the edge-reconstructed zGNRs can be recovered to those of the joint systems with perfect narrow H-terminated zGNRs through this hydrogenation pattern.

We selected the continuous 57-reconstruction at the zGNR edges as typical examples since it has drastical impacts on the electronic and magnetic properties of the joint systems, even can completely eliminate the magnetism of the joint systems based on zGNRs with both edges fully 57-reconstructed.

Here we investigated the joint systems of NO_2-(1)PDA-NH_2 and partially hydrogenated (denoted by "*p*H") zGNRs at both the fully 57-reconstructed edges, *p*H-N_z-zGNR-*f*57D, with series of widths (N_z = 12, 14, 16, even 18). As illustrated in **Figure 7**a, *p*H-*12*-zGNR-*f*57D exhibits typical half-metallic behavior with AFM state, similar to the joint system of NO_2-(1)PDA-NH_2 and the corresponding narrow H-*8*-zGNR with smooth edges, as discussed above. This indicates that partial hydrogenation can eliminate the effect of the edge reconstruction, and further, recover the electronic and magnetic features of the joint system with edge 57-reconstructed zGNR to those of the joint system with the corresponding narrow perfect H-terminated zGNR.

When the ribbon width is increased to 14, although the AFM half-metallic characteristic is sustained in *p*H-*14*-zGNR-*f*57D (Figure 7b), the profile of the band structure is also much similar to that of the corresponding joint system of NO_2-(1)PDA-NH_2 and the correlative narrow H-*10*-zGNR. With further widening the zGNR into 16-zGNR, even 18-zGNR, the half-metallic feature of the joint system is transformed into SGS in *p*H-*16*-zGNR-*f*57D and *p*H-*18*-zGNR-*f*57D due to the spatial decay of the induced dipole field, as illustrated in Figure 7c,d, whereas the AFM state is kept, analogous to the corresponding joint systems with their correlative narrow H-*12*-zGNR and H-*14*-zGNR, respectively. According to the computed DOSs of these four joint systems, the half-metallic behaviors in *p*H-*12*-zGNR-*f*57D and *p*H-*14*-zGNR-*f*57D mainly arise from the edge C atoms of the remaining perfect zGNR inside the partially hydrogenated zGNR at the NO_2 side of PDA, whereas it is the edge state of the edge C atoms of the remaining pristine zGNR inside and the impurity state of PDA that contribute to the SGS features of *p*H-*16*-zGNR-*f*57D and *p*H-*18*-zGNR-*f*57D, similar to the cases of the corresponding joint systems with the correlative narrow perfect zGNRs. This also supports the similarities of the electronic and magnetic properties between the joint systems based on partially hydrogenated zGNRs with both edges fully 57-reconstructed and on perfect H-terminated zGNRs.

Notably, partially hydrogenating zGNRs at the edges can eliminate the effect of the edge reconstruction, and further, generally recover the electronic and magnetic properties of the joint systems of PDA and wider zGNRs with both edges fully 57-reconstructed to those of the joint systems based on the corresponding narrow perfect zGNRs, resulting in the similar intriguing trend of half-metal–SGS and the preserved AFM state.

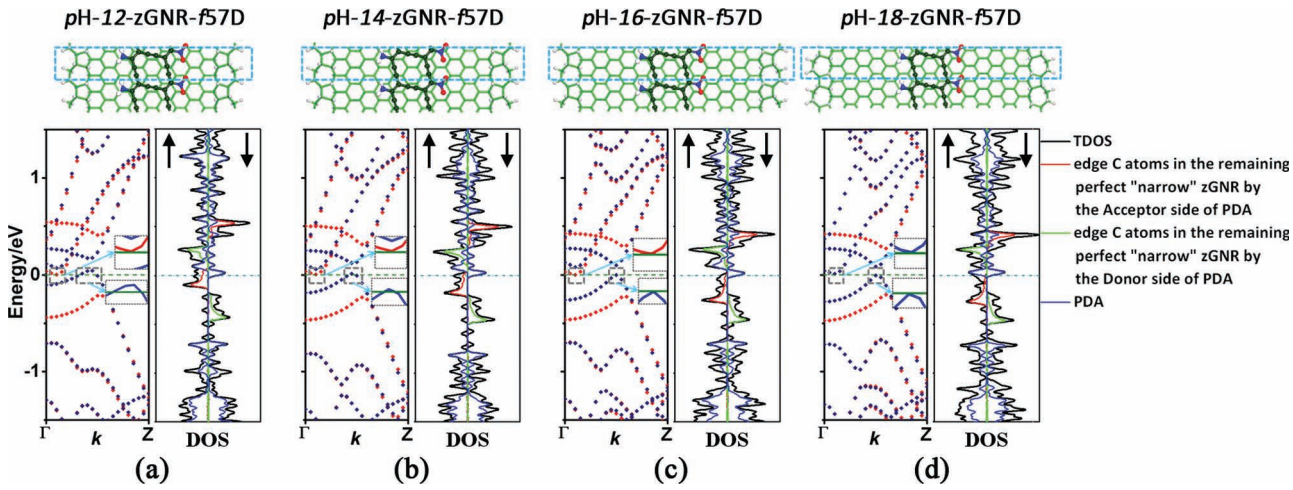

Figure 7. Equilibrium geometries, band structures and DOSs of the joint systems of NO_2-(1)PDA-NH_2 and partially hydrogenated zGNRs at both fully 57-reconstructed edges with series of widths (N_z = 12, 14, 16, 18). The blue and red plots denote the spin-up (↑) and spin-down (↓) channels for the band structures, respectively. The Fermi level is set as zero and marked with a green dashed line. The band behaviors about the Fermi-level are zoomed in to make them clearer. The parts in the blue dotted line correspond to one unit cell.

Clearly, partially hydrogenating zGNRs at the 57-reconstructed edges can serve as an effective approach to retain the intriguing half-metallic and SGS behaviors, as well as the electronic and magnetic property transitions in the joint systems of PDA and zGNRs with 57-reconstructed edges, thus is a very promising strategy for promoting more practical applications of zGNRs in the multi-functional and spintronic nanodevices.

2.3. The Stabilities of the Joint Systems Constructed by Depositing the PDA Derivatives on zGNRs

To examine the feasibility of experimental implementation, we computed the formation energies of the joint systems under study (**Tables** 1, 2, **3** and **4**). All these systems have negative formation energies, indicating that they are exothermic by depositing PDA derivatives on zGNRs with perfect, 57-reconstructed, and partially hydrogenated edge patterns, so they can be energetically favorable at common experimental conditions. Note that in the sampled joint systems *n*-NO_2-(*m*)PDA-NH_2, the formation energy decreases with increasing the –C≡C– number in the PDA derivatives. Such enhanced stability can be attributed to the more –C≡C– bonds, the more delocalized π-conjugation, and the stronger π–π interactions between PDA and zGNR, although the π–π interaction is different from those in the stacked hexagonal graphenes/benzenes layers. This is quite advantageous for experimental realization of the systems with more –C≡C– bonds in linking bridges.

Table 3. The relative energies (meV) of different magnetic couplings to the ground state per unit, formation energies (meV) per unit, and corresponding electronic properties of the joint systems of *n*-NO_2-(*m*)PDA-NH_2 (*n* = 8, 10, 12, 14; *m* = 1, 2, 3), respectively.

System	NM [meV]	FM [meV]	AFM [meV]	E_f [meV]	Electronic property
8-NO_2-(*1*)PDA-NH_2	98.0	16.4	0.0	–815.5	half-metal
8-NO_2-(*2*)PDA-NH_2	93.6	9.9	0.0	–953.4	half-metal
8-NO_2-(*3*)PDA-NH_2	97.1	0.0	6.0	–989.7	metal
10-NO_2-(*1*)PDA-NH_2	125.1	10.3	0.0	–890.5	SGS
10-NO_2-(*2*)PDA-NH_2	117.2	7.5	0.0	–941.1	half-metal
10-NO_2-(*3*)PDA-NH_2	126.2	0.0	5.5	–1090.7	metal
12-NO_2-(*1*)PDA-NH_2	146.0	5.1	0.0	–851.0	SGS
12-NO_2-(*2*)PDA-NH_2	128.4	4.2	0.0	–979.0	SGS
12-NO_2-(*3*)PDA-NH_2	127.5	0.0	18.0	–1090.5	metal
14-NO_2-(*1*)PDA-NH_2	138.5	3.8	0.0	–876.7	SGS
14-NO_2-(*2*)PDA-NH_2	129.6	2.7	0.0	–943.3	SGS
14-NO_2-(3)PDA-NH_2	134.6	1.7	0.0	–1093.8	metal

3. Conclusions

We have presented a new strategy, namely through the floating induced dipole field attached to zGNRs via π–π interactions, to effectively modulate the electronic and magnetic properties of zGNRs by means of DFT computations. This dipole field is induced by the acceptor/donor functional groups bridging ladder-structure polydiacetylene (PDA) derivatives with an excellent delocalized π-conjugated backbone.

Excitingly, a series of intriguing transitions of the electronic and magnetic features have been observed in the joint structures with the decorated PDA derivatives depositing on zGNRs with perfect, 57-reconstructed, and partially hydrogenated edge patterns. 1) The semiconducting H-terminated 8-zGNR can be driven into half-metal or metal with PDA derivatives decorated by several pairs of typical acceptor/donor groups (NO_2/NH_2, F/H, Cl/H, or CN/CH_3). Further, the transition of spin gapless semiconductor (SGS)–half-metal–metal and the magnetic conversion from AFM to FM

Table 4. The ground states, formation energies (meV) per unit and corresponding electronic properties of the joint systems based on bare 14-zGNR with four typical patterns of 57-reconstruction; H-terminated 14-zGNR with four typical patterns of 57-reconstruction; partially hydrogenated zGNRs at both fully 57-reconstructed edges with series of widths (N_z = 12, 14, 16, 18).

System	Ground state	E_f [meV]	Electronic property
eb-*14*-zGNR-*i*57S	FM	−917.6	half-metal
eb-*14*-zGNR-*i*57D	AFM	−912.6	SGS
eb-*14*-zGNR-*f*57S	AFM	−883.2	metal
eb-*14*-zGNR-*f*57D	NM	−878.9	metal
*e*H-*14*-zGNR-*i*57S	AFM	−907.3	metal
*e*H-*14*-zGNR-*i*57D	FM	−909.6	metal
*e*H-*14*-zGNR-*f*57S	AFM	−874.4	metal
*e*H-*14*-zGNR-*f*57D	NM	−889.3	metal
*p*H-*12*-zGNR-*f*57D	AFM	−825.4	half-metal
8-NO_2-(*1*)PDA-NH_2	AFM	−815.5	half-metal
*p*H-*14*-zGNR-*f*57D	AFM	−897.3	half-metal
10-NO_2-(*1*)PDA-NH_2	AFM	−890.5	SGS
*p*H-*16*-zGNR-*f*57D	AFM	−855.0	SGS
12-NO_2-(*1*)PDA-NH_2	AFM	−851.0	SGS
*p*H-*18*-zGNR-*f*57D	AFM	−847.5	SGS
14-NO_2-(*1*)PDA-NH_2	AFM	−876.7	SGS

can be endowed by narrowing/widening the width of zGNR or increasing the number of –C≡C– bonds in the linking bridge of the NO_2/NH_2 decorating PDA derivatives. 2) When the edge 57-reconstructions occur, abundant electronic and magnetic transitions of AFM SGS–FM half-metal–AFM metal–NM metal can also be achieved in the joint systems. 3) Partially hydrogenating zGNRs at the 57-reconstructed edges is an effective and promising approach to eliminate the effect of the edge reconstruction, and to generally recover the electronic and magnetic properties of the joint systems based on the edge-reconstructed zGNRs to those of the corresponding joint structures with perfect narrow H-terminated zGNRs. A similar intriguing trend of half-metallicity–SGS can also be achieved in the partially hydrogenated joint systems based on wider edge-reconstructed zGNRs.

Our concepts provide simple and effective approaches for experimentally realizing not only half-metallicity and spin gapless semiconductor but also the abundant electronic and magnetic transitions in the zGNR-based nanostructures. Note that all of the joint systems investigated in this work are energetically favorable. We are highly anticipating that these fascinating findings would further advance the theoretical design and the experimental actualization of zGNR-based multi-functional and spintronic nanodevices in the very near future.

4. Computational Methods

The generalized gradient approximation (GGA) with the Perdew-Burke-Ernzerhof exchange-correlation functional[88] (including a semiempirical van der Waals (vdW) correction to account for the dispersion interactions)[89,90] and a 400 eV cutoff for the plane-wave basis set were used to perform all the density-functional theory (DFT) computations within the frame of Vienna ab initio simulation package (VASP).[91–94] The projector-augmented plane wave (PAW)[95,96] was used to describe the electron-ion interactions. Vacuum spaces of wider than 15 Å were adopted along the nonperiodical directions to ensure that the spurious interactions between the images in the repeated supercells are negligible. 1 × 1 × 10 Monkhorst-Pack grid *k*-points were employed for geometric optimization, and the convergence threshold was set as 10^{-4} eV in energy and 10^{-3} eV Å^{-1} in force. To further investigate the electronic behaviors, 21 uniform *k*-points were utilized for sampling the 1D Brillouin zone. For evaluating the stability of the joint systems, the following equation was defined to estimate the formation energies (E_f):

$$E_f = E_{zGNR+PDA} - (E_{zGNR} + E_{PDA}) \quad (1)$$

where $E_{zGNR+PDA}$, E_{zGNR}, and E_{PDA} are the total energies of the joint systems, zGNRs and the decorated PDA derivatives, respectively. According to this definition, negative formation energies indicate the exothermic (energetically favorable) process for depositing PDA derivatives on zGNRs. Note that for the joint systems of PDA and zGNRs with edges partially 57-reconstructed, in which the size of the supercells is twice as large as that of others, the corresponding formation energies are divided by two for comparison.

Acknowledgements

This work was supported in China by the National Basic Research Program of China (973 Program) (2012CB932800), NSFC (21103065, 21073075 and 21173097), and the Ministry of Education of China (20110061120024 and 20100061110046), and in the USA by the Department of Defense (Grant W911NF-12-1-0083) and partially by the NSF (Grant EPS-1010094). G.T.Y. and W.C. are grateful for equipment funds (450091105163 and 450091105164) and funds (450060481347, 450080011085, and 450080011084) from Jilin University. The authors acknowledge the High Performance Computing Center (HPCC) of Jilin University for supercomputer time.

Received: June 20, 2012
Revised: August 20, 2012
Published online: October 26, 2012

[1] K. S. Novoselov, A. K. Geim, S. V. Morozov, D. Jiang, Y. Zhang, S. V. Dubonos, I. V. Grigoreva, A. A. Firsov, *Science* **2004**, *306*, 666.
[2] K. S. Novoselov, D. Jiang, F. Schedin, T. J. Booth, V. V. Khotkevich, S. V. Morozov, A. K. Geim, *Proc. Natl. Acad. Sci. USA* **2005**, *102*, 10451.
[3] M. J. Allen, V. C. Tung, R. B. Kaner, *Chem. Rev.* **2010**, *110*, 132.
[4] A. K. Geim, K. S. Novoselov, *Nat. Mater.* **2007**, *6*, 183.
[5] J. A. Rogers, *Nat. Nanotechnol.* **2008**, *3*, 254.
[6] G. Brumfiel, *Nature* **2009**, *458*, 390.
[7] D. Li, R. B. Kaner, *Science* **2008**, *320*, 1170.
[8] R. F. Service, *Science* **2009**, *324*, 875.

[9] L. A. Ponomarenko, F. Schedin, M. I. Katsnelson, R. Yang, E. W. Hill, K. S. Novoselov, A. K. Geim, *Science* **2008**, *320*, 356.
[10] C. Berger, Z. Song, X. Li, X. Wu, N. Brown, C. Naud, D. Mayou, T. Li, J. Hass, A. N. Marchenkov, E. H. Conrad, P. N. First, W. A. d. Heer, *Science* **2006**, *312*, 1191.
[11] M. I. Katsnelson, K. S. Novoselov, A. K. Geim, *Nat. Phys.* **2006**, *2*, 620.
[12] M. I. Katsnelson, K. S. Novoselov, *Solid State Commun.* **2007**, *143*, 3.
[13] K. S. Novoselov, Z. Jiang, Y. Zhang, S. V. Morozov, H. L. Stormer, U. Zeitler, J. C. Maan, G. S. Boebinger, P. Kim, A. K. Geim, *Science* **2007**, *315*, 1379.
[14] Y. Zhang, Y.-W. Tan, H. L. Stormer, P. Kim, *Nature* **2005**, *438*, 201.
[15] S. V. Morozov, K. S. Novoselov, M. I. Katsnelson, F. Schedin, D. Elias, J. A. Jaszczak, A. K. Geim, *Phys. Rev. Lett.* **2008**, *100*, 016602.
[16] G. Lee, X. Wei, J. W. Kysar, J. Hone, *Science* **2008**, *321*, 385.
[17] S. M. Kozlov, F. Viñes, A. Görling, *Adv. Mater.* **2011**, *23*, 2638.
[18] D. C. Elias, R. R. Nair, T. M. G. Mohiuddin, S. V. Morozov, P. Blake, M. P. Halsall, A. C. Ferrari, D. W. Boukhvalov, M. I. Katsnelson, A. K. Geim, K. S. Novoselov, *Science* **2009**, *323*, 610.
[19] D. W. Boukhvalov, M. I. Katsnelson, *Nano Lett.* **2008**, *8*, 4373.
[20] A. K. Singh, B. I. Yakobson, *Nano Lett.* **2009**, *9*, 1540.
[21] N. Lu, Z. Y. Li, J. L. Yang, *J. Phys. Chem. C* **2009**, *113*, 16741.
[22] J.-H. Chen, W. G. Cullen, C. Jang, M. S. Fuhrer, E. D. Williams, *Phys. Rev. Lett.* **2009**, *102*, 236805.
[23] A. Hashimoto, K. Suenaga, A. Gloter, K. Urita, S. Iijima, *Nature* **2004**, *430*, 870.
[24] S. Zhou, G. H. Gweon, A. V. Fedorov, P. N. First, W. A. de Heer, D. H. Lee, F. Guinea, A. H. Neto, A. Lanzara, *Nat. Mater.* **2007**, *6*, 770.
[25] W. Chen, S. Chen, D. C. Qi, X. Y. Gao, A. T. S. Wee, *J. Am. Chem. Soc.* **2007**, *129*, 10418.
[26] A. J. Du, S. C. Smith, *J. Phys. Chem. Lett.* **2011**, *2*, 73.
[27] A. J. Du, S. Sanvito, Z. Li, D. W. Wang, Y. Jiao, T. Liao, Q. Sun, Y. H. Ng, Z. H. Zhu, R. Amal, S. C. Smith, *J. Am. Chem. Soc.* **2012**, *134*, 4393.
[28] X. T. Jia, J. Campos-Delgado, M. Terrones, V. Meunier, M. S. Dresselhaus, *Nanoscale* **2011**, *3*, 86.
[29] A. R. Botello-Méndez, E. Cruz-Silva, J. M. Romo-Herrera, F. López-Urías, M. Terrones, B. G. Sumpter, H. Terrones, J. -C. Charlier, V. Meunier, *Nano Lett.* **2011**, *11*, 3058.
[30] K. Nakada, M. Fujita, G. Dresselhaus, M. S. Dresselhaus, *Phys. Rev. B* **1996**, *54*, 17954.
[31] M. Fujita, K. Wakabayashi, K. Nakada, K. Kusakabe, *J. Phys. Soc. Jpn.* **1996**, *65*, 1920.
[32] K. Wakabayashi, M. Sigrist, M. J. Fujita, *J. Phys. Soc. Jpn.* **1998**, *67*, 2089.
[33] K. Wakabayashi, M. Fujita, H. Ajiki, M. Sigrist, *Phys. Rev. B* **1999**, *59*, 8271.
[34] Y.-W. Son, M. L. Cohen, S. G. Louie, *Phys. Rev. Lett.* **2006**, *97*, 216803.
[35] D. E. Jiang, B. G. Sumpter, S. Dai, *J. Chem. Phys.* **2007**, *127*, 124703.
[36] V. Barone, O. Hod, G. E. Scuseria, *Nano Lett.* **2006**, *6*, 2748.
[37] X. L. Li, X. R. Wang, L. Zhang, S. W. Lee, H. J. Dai, *Science* **2008**, *319*, 1229.
[38] K. A. Ritter, J. W. Lyding, *Nat. Mater.* **2009**, *8*, 235.
[39] K. N. Kudin, *ACS Nano* **2008**, *2*, 516.
[40] Y.-W. Son, M. L. Cohen, S. G. Louie, *Nature* **2006**, *444*, 347.
[41] T. Wassman, A. P. Seitsonen, A. M. Saitta, M. Lazzeri, F. Mauri, *Phys. Rev. Lett.* **2008**, *101*, 096402.
[42] D. E. Jiang, B. G. Sumpter, S. Dai, *J. Chem. Phys.* **2007**, *126*, 134701.
[43] H. Hiura, *Appl. Surf. Sci.* **2004**, *222*, 374.
[44] K. S. Novoselov, A. K. Geim, S. V. Morozov, D. Jiang, M. I. Katsnelson, I. V. Grigorieva, S. V. Dubonos, A. A. Firsov, *Nature* **2005**, *438*, 197.
[45] M. Terrones, A. R. Botello-Méndez, J. Campos-Delgado, F. Lopez-Urías, Y. I. Vega-Cantú, F. J. Rodríguez-Macías, A. L. Elías, E. Muñoz-Sandoval, A. G. Cano-Márquez, J.-C. Charlier, H. Terrones, *Nano Today* **2010**, *5*, 351.
[46] S. Dutta, S. K. Pati, *J. Mater. Chem.* **2010**, *20*, 8207.
[47] Y. F. Li, Z. Zhou, P. W. Shen, Z. F. Chen, *J. Phys. Chem. C* **2009**, *113*, 15043.
[48] H. Xiang, E. Kan, S.-H. Wei, N.-H. Whangbo, J. Yang, *Nano Lett.* **2009**, *9*, 4025.
[49] S. Dutta, S. K. Pati, *Carbon* **2010**, *48*, 4409.
[50] L. L. Song, X. H. Zheng, R. L. Wang, Z. Zeng, *J. Phys. Chem. C* **2010**, *114*, 12145.
[51] J. Kunstmann, C. Özdoğan, A Quandt, H. Fehske, *Phys. Rev. B* **2011**, *83*, 045414.
[52] X. L. Wang, *Phys. Rev. Lett.* **2008**, *100*, 156404.
[53] X. L. Wang, S. X. Dou, C. Zhang, *NPG Asia Mater.* **2010**, *2*, 31.
[54] K. J. Lee, S. M. Choo, J. B. Yoon, K. M. Song, Y. Saiga, C.-Y. You, N. Hur, S. I. Lee, T. Takabatake, M. H. Jung, *J. Appl. Phys.* **2010**, *107*, 09C306.
[55] S. W. Chen, S. C. Huang, G. Y. Guo, J. M. Lee, S. Chiang, W. C. Chen, Y. C. Liang, K. T. Lu, J. M. Chen, *Appl. Phys. Lett.* **2011**, *99*, 012103.
[56] Y. F. Li, Z. Zhou, P. W. Shen, Z. F. Chen, *ACS Nano* **2009**, *3*, 1952.
[57] E. J. Kan, Z. Y. Li, J. L. Yang, J. G. Hou, *J. Am. Chem. Soc.* **2008**, *130*, 4224.
[58] M. H. Wu, X. J. Wu, X. C. Zeng, *J. Phys. Chem. C* **2010**, *114*, 3937.
[59] S. Dutta, S. K. Pati, *J. Phys. Chem. B* **2008**, *112*, 1333.
[60] O. Hod, V. Barone, J. E. Peralta, G. E. Scuseria, *Nano Lett.* **2007**, *7*, 2295.
[61] M. H. Wu, X. J. Wu, Y. Gao, X. C. Zeng, *Appl. Phys. Lett.* **2009**, *94*, 223111.
[62] X. H. Zheng, X. L. Wang, T. A. Abtew, Z. Zeng, *J. Phys. Chem. C* **2010**, *114*, 4190.
[63] S. Dutta, A. K. Manna, S. K. Pati, *Phys. Rev. Lett.* **2009**, *102*, 096601.
[64] X. Lin, J. Ni, *Phys. Rev. B* **2011**, *84*, 075461.
[65] Y. L. Liu, X. J. Wu, Y. Zhao, X. C. Zeng, J. L. Yang, *J. Phys. Chem. C* **2011**, *115*, 9442.
[66] H. Park, J. Y. Lee, S. Shin, *J. Phys. Chem. C* **2012**, *116*, 20054..
[67] Z. Y. Li, B. Huang, W. H. Duan, *J. Nanosci. Nanotechnol.* **2010**, *10*, 5374.
[68] Y. L. Lee, S. Kim, C. Park, J. Ihm, Y. W. Son, *ACS Nano* **2010**, *4*, 1345.
[69] S. D. Dalosto, Z. H. Levine, *J. Phys. Chem. C* **2008**, *112*, 8196.
[70] A. Nduwimana, X.-Q. Wang, *ACS Nano* **2009**, *3*, 1995.
[71] G. Wegner, *Z. Naturforsch.* **1969**, *24b*, 824.
[72] S. Okada, K. Hayamizu, H. Matsuda, A. Masaki, N. Minami, H. Nakanishi, *Macromolecules* **1994**, *27*, 6259.
[73] H. Matsuzawa, S. Okada, H. Matsuda, H. Nakanishi, *Proc. SPIE* **1996**, *2851*, 14.
[74] S. Okada, H. Nakanishi, H. Matsuzawa, H. Katagi, T. Oshikiri, H. Kasai, A. Sarkar, H. Oikawa, R. Rangel-Rojo, T. Fukuda, H. Matsuda, *Proc. SPIE* **1999**, *3796*, 76.
[75] S. Inayama, Y. Tatewaki, S. Okada, *Polym. J.* **2010**, *42*, 201.
[76] J. J. Liang, L. Huang, N. Li, Y. Huang, Y. P. Wu, S. L. Fang, J. Oh, M. Kozlov, Y. F. Ma, F. F. Li, R. Baughman, Y. S. Chen, *ACS Nano* **2012**, *6*, 4508.
[77] M. Akai-Kasaya, Y. Yamamoto, A. Saito, M. Aono, Y. Kuwahara, *Jpn. J. Appl. Phys.* **2006**, *45*, 2049.
[78] M. Akai-Kasaya, K. Shimizu, A. Saito, M. Aono, Y. Kuwahara, *Phys. Rev. Lett.* **2003**, *91*, 255501.
[79] R. Giridharagopal, K. F. Kelly, *ACS Nano* **2008**, *2*, 1571.
[80] W. Chen, G. T. Yu, F. L. Gu, Y. Aoki, *Chem. Phys. Lett.* **2009**, *474*, 175.

[81] P. Koskinen, S. Malola, H. Häkkinen, *Phys. Rev. B* **2009**, *80*, 073401.
[82] Ç. Ö. Girit, J. C. Meyer, R. Erni, M. D. Rossell, C. Kisielowski, L. Yang, C-H. Park, M. F. Crommie, M. L. Cohen, S. G. Louie, A. Zettl, *Science* **2009**, *323*, 1705.
[83] A. Chuvilin, J. C. Meyer, G. Algara-Siller, U. Kaiser, *New J. Phys.* **2009**, *11*, 083019.
[84] P. Koskinen, S. Malola, H. Häkkinen, *Phys. Rev. Lett.* **2008**, *101*, 115502.
[85] L. T. Nguyen, C. H. Pham, V. L. Nguyen, *J. Phys.: Condens. Matter* **2011**, *23*, 295503.
[86] J. M. H. Kroes, M. A. Akhukov, J. H. Los, N. Pineau, A. Fasolino, *Phys. Rev. B* **2011**, *83*, 165411.
[87] B. Huang, M. Liu, N. Su, J. Wu, W. Duan, B.-l. Gu, F. Liu, *Phys. Rev. Lett.* **2009**, *102*, 166404.
[88] J. P. Perdew, K. Burke, M. Ernzerhof, *Phys. Rev. Lett.* **1996**, *77*, 3865.
[89] S. J. Grimme, *Comput. Chem.* **2006**, *27*, 1787.
[90] X. Wu, M. C. Vargas, S. Nayak, V. Lotrich, G. Scoles, *J. Chem. Phys.* **2001**, *115*, 8748.
[91] G. Kresse, J. Hafner, *Phys. Rev. B* **1993**, *47*, 558.
[92] G. Kresse, J. Hafner, *Phys. Rev. B* **1994**, *49*, 14251.
[93] G. Kresse, J. Furthmuller, *Comput. Mater. Sci.* **1996**, *6*, 15.
[94] G. Kresse, J. Furthmuller, *Phys. Rev. B* **1996**, *54*, 11169.
[95] P. E. Blochl, *Phys. Rev. B* **1994**, *50*, 17953.
[96] G. Kresse, D. Joubert, *Phys. Rev. B* **1999**, *59*, 1758.